

Split Photosystem Protein, Linear-Mapping Topology, and Growth of Structural Complexity in the Plastid Genome of *Chromera velia*

Jan Janouškovec,^{*†,1} Roman Sobotka,^{†,2,3} De-Hua Lai,^{†,‡,4} Pavel Flegontov,⁴ Peter Koník,³ Josef Komenda,^{2,3} Shahjahan Ali,⁵ Ondřej Prášil,^{2,3} Arnab Pain,⁶ Miroslav Oborník,^{2,3,4} Julius Lukeš,^{3,4} and Patrick J. Keeling^{*1}

¹Department of Botany, University of British Columbia, Vancouver, British Columbia, Canada

²Institute of Microbiology, Czech Academy of Sciences, Třeboň, Czech Republic

³Faculty of Science, University of South Bohemia, České Budějovice, Czech Republic

⁴Biology Centre, Institute of Parasitology, Czech Academy of Sciences, České Budějovice, Czech Republic

⁵Biosciences Core Laboratory-Genomics, King Abdullah University of Science and Technology (KAUST), Thuwal, Kingdom of Saudi Arabia

⁶Computational Bioscience Research Center (CBRC), King Abdullah University of Science and Technology (KAUST), Thuwal, Kingdom of Saudi Arabia

[†]These authors contributed equally to this work.

[‡]Present address: School of Life Sciences, Sun Yat-Sen University, Guangzhou, China

***Corresponding author:** E-mail: janjan.cz@gmail.com; pkeeling@mail.ubc.ca.

Associate editor: Charles Delwiche

Abstract

The canonical photosynthetic plastid genomes consist of a single circular-mapping chromosome that encodes a highly conserved protein core, involved in photosynthesis and ATP generation. Here, we demonstrate that the plastid genome of the photosynthetic relative of apicomplexans, *Chromera velia*, departs from this view in several unique ways. Core photosynthesis proteins PsA and AtpB have been broken into two fragments, which we show are independently transcribed, oligoU-tailed, translated, and assembled into functional photosystem I and ATP synthase complexes. Genome-wide transcription profiles support expression of many other highly modified proteins, including several that contain extensions amounting to hundreds of amino acids in length. Canonical gene clusters and operons have been fragmented and reshuffled into novel putative transcriptional units. Massive genomic coverage by paired-end reads, coupled with pulsed-field gel electrophoresis and polymerase chain reaction, consistently indicate that the *C. velia* plastid genome is linear-mapping, a unique state among all plastids. Abundant intragenomic duplication probably mediated by recombination can explain protein splits, extensions, and genome linearization and is perhaps the key driving force behind the many features that defy the conventional ways of plastid genome architecture and function.

Key words: plastid genome evolution, *Chromera velia*, split protein, linear-mapping genome.

Introduction

Chromera velia is an autotrophic alveolate that was discovered during a survey of zooxanthellae in Australian coral reefs (Moore et al. 2008). The dominant reef symbionts are dinoflagellates from the genus *Symbiodinium*, but *C. velia* was found to be related to the sister group of dinoflagellates, the apicomplexan parasites (Moore et al. 2008; Oborník et al. 2009). Because apicomplexans include a number of medically and economically important pathogens (e.g., the malaria parasite *Plasmodium*, as well as *Toxoplasma*, *Cryptosporidium*, and *Babesia*), and because of the interest in the cryptic, non-photosynthetic plastid that has now been found in many of these apicomplexans, the nature of the plastid in *C. velia* was of immediate interest. Accordingly, the complete *C. velia* plastid genome was characterized and

has proven critical in elucidating the origin of the apicomplexan plastid and its relationship to that of dinoflagellates (Janouškovec et al. 2010), and other plastid-related metabolic pathways have also already been compared with those of apicomplexans (Botté et al. 2011; Kořený et al. 2011).

Although these questions have certainly directed much attention to *C. velia* and its plastid in particular, they have also overshadowed the intrinsic interest in this organism. Aside from being a key to understanding apicomplexan plastids, *C. velia* is itself potentially interesting and important both ecologically and evolutionarily (Janouškovec et al. 2012). This is because *C. velia* is one of the few known photosynthetic lineages in the alveolates (the others being *Vitrella* and dinoflagellates; Oborník et al. 2012), so its plastid represents new breadth in the study of plastid diversity never before

accessible for comparison with other plastids. Indeed, the initial description of the *C. velia* plastid genome noted several unusual features with implications for plastid evolution and function (Janouškovec et al. 2010), but because they were typically not shared with either apicomplexans or dinoflagellates (and therefore not comparable to them), they have not been characterized further.

Here, we describe three intriguing features of the *C. velia* plastid genome: the presence of split genes encoding split proteins, divergent characteristics of gene organization and expression, and the physical structure of the chromosome. We show that two functionally important proteins involved in photosynthesis, PsaA representing a core subunit of photosystem I (PSI) and AtpB representing the beta subunit of the ATP synthase, are expressed in two discrete fragments at both the RNA and protein levels, which has interesting implications for the structure and function of these otherwise highly conserved proteins. We also show that the plastid chromosome is highly divergent in structure with a pronounced strand polarity, altered gene order, and large extensions in many coding sequences, which appear transcribed. Finally, we significantly expand the depth of sequence coverage at the DNA level, and show that the coverage pattern at the chromosome ends, polymerase chain reaction (PCR) experiments, genome migration on pulse field gels, and presence of two long terminal inverted repeats (TIRs) all suggest that the genome is linear in structure. This would represent the first documented case of a linear-mapping plastid genome. These unique characteristics substantially expand our current understanding of plastid genome diversity, much of which we hypothesize is due to high levels of intra-genomic duplication in this lineage.

Results

Fragmented Genes Encode Fragmented Proteins Expressed from Polycistronic mRNAs

The complete *C. velia* plastid genome contained a number of small fragments of genes, including *psaA*, *atpB*, *psaB*, *psbB*, *rpl3*, and *tufA*. In most of these cases, intact homologs were also present, but in *psaA* and *atpB* only two fragments were found that were widely separated in the genome and that together would account for the entire gene (*psaA*-1, *psaA*-2, *atpB*-1, and *atpB*-2). Both gene products are critical for photosynthesis and ATP generation, suggesting three possible explanations, all of which are unusual: the plastid fragments are pseudogenes and intact proteins are imported from the cytosol, the plastid gene products are *trans*-spliced at the RNA or protein levels, or the proteins function as unique two-subunit forms.

Expression of *psaA*-1 and *psaA*-2 fragments was examined by transcript mapping by circularizing mRNAs and Northern analysis (see Materials and Methods). Reverse transcriptase RT-PCR on circularized mRNA produced a product from each of the fragments comprising the coding region, flanking sequence, and a short 6–12 nucleotide-long oligouridylylated (oligoU) tail (fig. 1). The consistent failure to connect the fragments by RT-PCR using multiple primer sets suggested

they are not spliced at the RNA level. Both *psaA*-1 and *psaA*-2 are surrounded by several genes on the same strand, so their co-ordinated expression was analyzed by hybridization to probes corresponding to *psaA*-1, *psaA*-2, the upstream genes, and the downstream noncoding region. All probes hybridized with a fragment of the expected size of a stand-alone oligoU mRNA corresponding to the fragment in question: no evidence for a spliced RNA form was found. However, probes did hybridize to larger fragments (fig. 1 and supplementary fig. S1, Supplementary Material online) corresponding in size and hybridization pattern to a single dicistronic (*psaA*-1 + *psbB*) or multiple large polycistronic mRNAs (*psaA*-2 + *psbE* + *psaB*, and surrounding genes). Linkages between *psaA*-1 and *psbB* and *psaA*-2 and *psaB* were confirmed by RT-PCR. Hybridization patterns around *psaA*-2 suggested processing of large mRNAs into the dicistronic *psaA*-2 + *psbE* and subsequently to single gene transcripts (fig. 1). Similar to *psaA*, all attempts to link the two *atpB* fragments by RT-PCR yielded no products. The Northern analysis of *atpB*-1 and *atpB*-2 revealed single bands corresponding in size to each expected fragment and no evidence was found for a spliced mRNA, again suggesting independent expression (fig. 2A). The transcriptional profiles of both *atpB* fragments were supportive of this conclusion (fig. 2B). All four *psaA* and *atpB* fragments contained structurally conserved domains (figs. 1 and 2A) and were among the top 22 most abundantly transcribed plastid genes (table 1, and see later). Evidence at the genomic and transcriptomic levels therefore consistently suggested that all *psaA* and *atpB* fragments are independently transcribed, translated, and code for functional products.

To obtain convincing evidence that *psaA* and *atpB* gene fragments are expressed as separate polypeptides, and that no intact version of the proteins is present, we analyzed membrane protein complexes by combination of two-dimensional (2D) electrophoresis and mass spectrometry (MS). Membrane fraction isolated from *C. velia* cells was solubilized by dodecyl- β -maltoside and protein complexes were separated on Clear-Native gel in the first dimension and on sodium dodecyl sulfate (SDS) gel in the second dimension (fig. 3). The most abundant spots were subjected to MS analysis of their tryptic peptides which were correlated with predicted peptides of plastid-encoded genes and available expressed sequence tag (EST) sequences. This allowed us to distinguish photosystem II (PSII), cytochrome b_6/f , and PSI and PSII supercomplexes with bound antennas (fig. 3). Fragments corresponding to PsaA-1, PsaA-2, AtpB-1, and AtpB-2 were all identified, but no spot with the expected mass/charge properties of intact PsaA and AtpB was found (see supplementary tables S1 and S2, Supplementary Material online, for a list of peptides assigned to PsaA/B and AtpA/B proteins). Identification of spots was consistent with chlorophyll fluorescence detected in the native gel. All three PSII complexes exhibited strong fluorescence, which contrasted with the minimal fluorescence of chlorophyll bound within the PSI supercomplex. The minimal fluorescence emission from the PSI complex indicated it was well preserved before it was separated into subunits in the second dimension

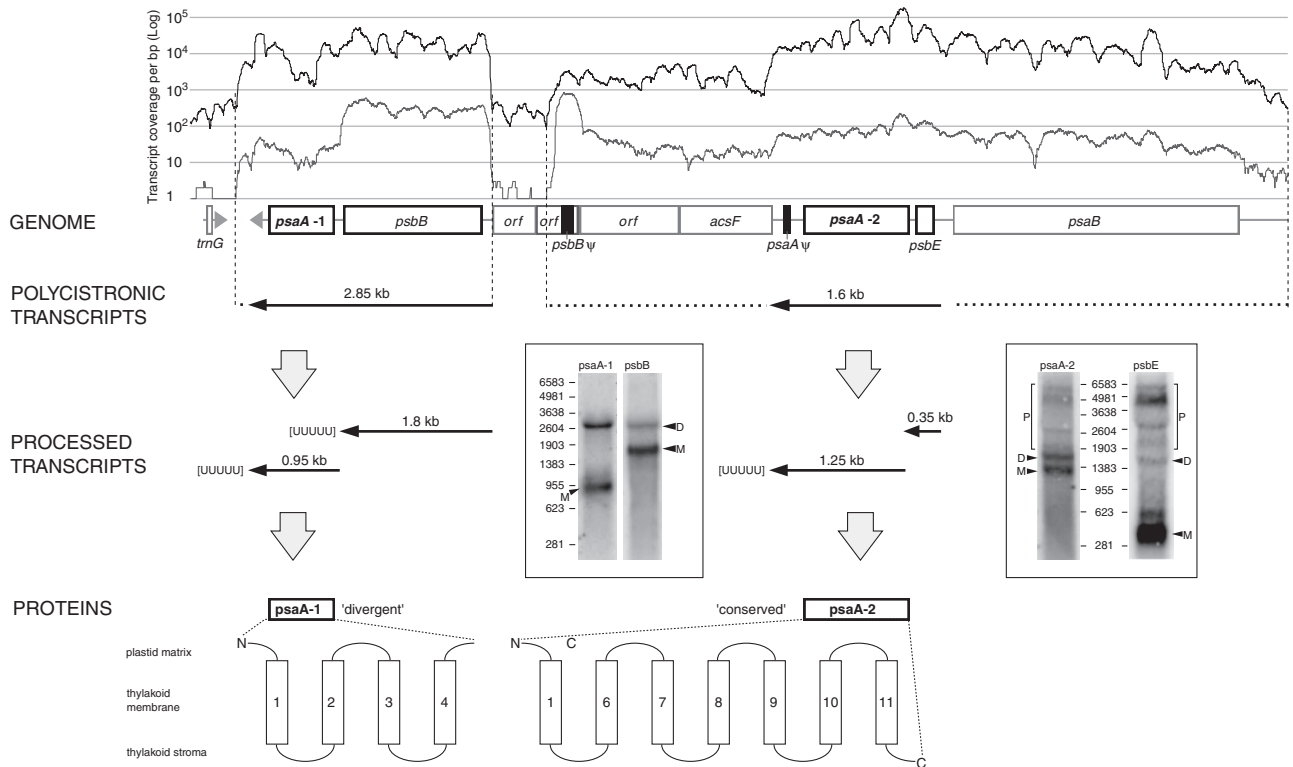


Fig. 1. Expression model for the split PsaA. PsaA fragments are separated at the genomic, transcriptomic, and protein level (top to bottom). The top graph shows the transcriptional profile (total RNA in black upper line and polyA RNA in gray lower line) of the genomic region below. In the genomic region, boxes represent genes and gray arrows show the coding DNA strand. Consistent with the transcriptional profile, Northern hybridization blots (boxes below) reveal that both *psaA* fragments are transcribed within larger polycistronic transcripts (P) and further processed into dicistronic (D) and monocistronic (M) units. The monocistronic *psaA* transcripts contain oligoU tails and translate into independent peptides both of which participate in PSI (thylakoid trans-membrane domains are shown by vertical boxes and numbered).

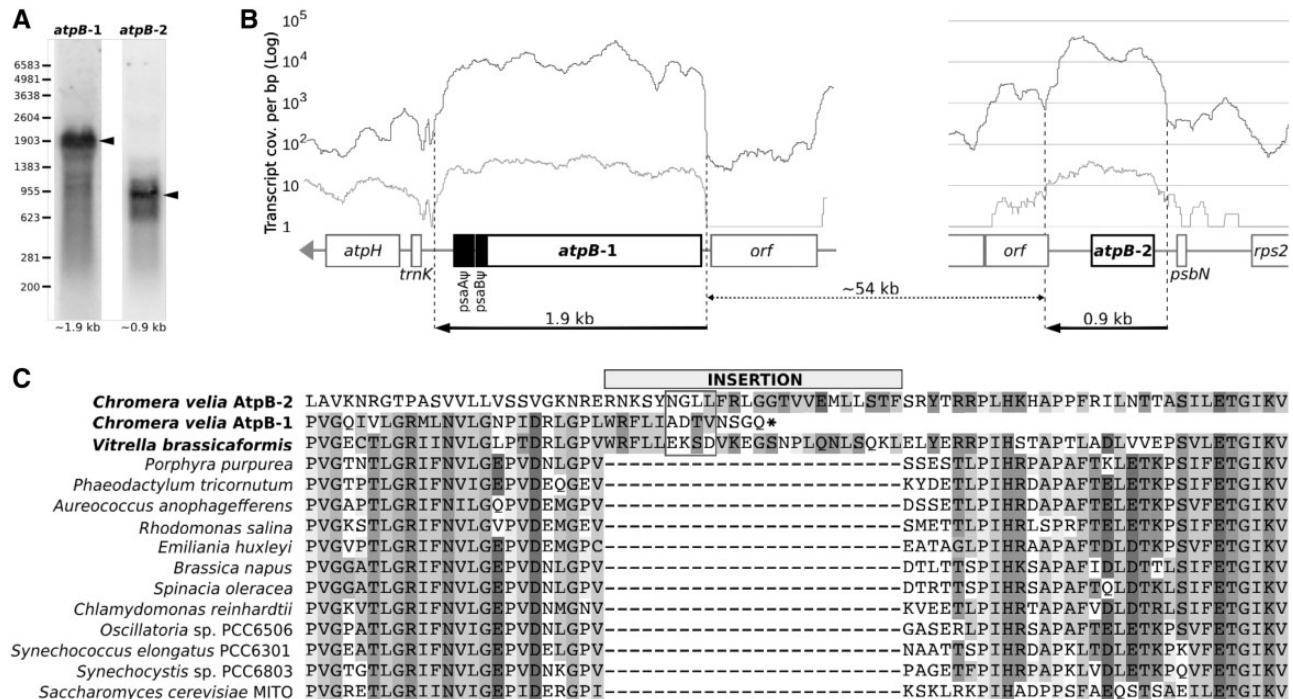


Fig. 2. Expression model for the split AtpB. (A) Northern analysis revealed a monocistronic transcript for each of the two *atpB* fragments. (B) Transcriptome coverage of the two genomic regions is shown for total RNA (black upper line) and polyA RNA (gray lower line). Genes are shown by boxes and gray arrows indicate coding strands. Black arrows below indicate predicted transcripts based on the combination of transcript mapping and Northern analysis. (C) Alignment of plastid, cyanobacterial, and yeast mitochondrial AtpBs reveals that the split of *Chromera velia* AtpB occurred within a 24 amino acid insertion that is also present in the sister taxon *Vitrella* (the most probable positions of the split are boxed).

Table 1. Total RNA Transcript Mapping to *Chromera velia* Plastid Genes.

Region	Number/Gene	Length (kb)	Cov/bp ^a	Rel. Cov. vs. Med. ^b
Intergenic regions ^c	105	22.4	3444	
Genes ^c	107	94.1	33990	
Ribosomal RNA	3	4.8	348584	475.3
Transfer RNA	29	2.4	699	1.0
Protein-coding	75	86.9	12033	16.4
Photosystem II (<i>psb</i>)	11	6.6	52244	71.2
Photosystem I (<i>psa</i>)	4	5.7	22740	31.0
Cytochrome b6/f (<i>pet</i>)	4	2.1	18301	25.0
ATP synthase (<i>atp</i>)	6	5.1	14762	20.1
Ribosomal proteins large subunit (<i>rrl</i>)	10	5.4	1141	1.6
Ribosomal proteins small subunit (<i>rrs</i>)	12	16.8	1328	1.8
Thylakoid import (<i>sec</i> , <i>tat</i>)	3	4.5	817	1.1
RNA polymerase (<i>rpo</i>)	4	15.4	293	0.4
Other function (<i>acsF</i> , <i>ccsA</i> , <i>clpC</i> , <i>tufA</i> , <i>ycf3</i>)	7	11.9	3617	4.9
Unknown function (<i>orf</i>)	14	13.5	1339	1.8
Highly expressed protein-coding genes	<i>psbA</i>	1.0	383384	522.8
	<u><i>psaA-2</i></u>	1.2	48594	66.3
	<i>psbE</i>	0.3	41694	56.9
	<i>atpH1</i>	0.2	41540	56.6
	<i>psbD</i>	1.0	37785	51.5
	<i>psbC</i>	1.4	32123	43.8
	<i>petD</i>	0.5	27882	38.0
	<i>psbB</i>	1.6	23102	31.5
	<i>psbV</i>	0.5	20686	28.2
	<i>psaC</i>	0.2	19422	26.5
	<i>atpA</i>	1.7	17239	23.5
	<i>petA</i>	0.9	16957	23.1
	<u><i>atpB-1</i></u>	0.5	15992	21.8
	<i>psbH</i>	0.3	15653	21.3
	<i>petB</i>	0.6	15341	20.9
	<i>psaB</i>	3.4	14407	19.6
	<i>tufA</i>	1.3	13235	18.0
	<i>petG</i>	0.1	13026	17.8
	<u><i>atpB-2</i></u>	1.5	10950	14.9
	<i>psbK</i>	0.1	9339	12.7
	<u><i>psaA-1</i></u>	0.8	8538	11.6
	<i>psbJ</i>	0.1	8027	10.9

NOTE.—Genes encoding split proteins are underlined.

^aAverage coverage per base pair.

^bRelative coverage compared with median gene coverage depth per base pair (=733.4).

^cGene/intergenic regions in the TIRs were counted once.

(fig. 3). This, together with the lack of evidence for intact genes or transcripts for either gene, suggested strongly that the two separate subunits of both PsaA and AtpB proteins are assembled into functional PSI and ATP synthase, respectively.

Modeling the two-subunit forms shows that the point at which both genes were split corresponds to a loop spanning structural domains (fig. 1). In the case of PsaA, the position of this breakpoint corresponds to the largest loop in the protein, which separates the first two pairs of peripheral helices from the rest of the protein including the photochemistry-performing core (fig. 1; Jordan et al. 2001; Green 2003). The split has also driven a considerable change in divergence rate between the two peptides: PsaA-

1 at the photosynthetic antenna periphery is significantly less conserved than PsaA-2 at the antenna core. By calculating maximum likelihood-corrected genetic distances (see Materials and Methods), we estimated that PsaA-1 is about 4.6 times more divergent than PsaA-2 relative to other plastid homologs, suggesting that it is, not surprisingly, under weaker functional constraint. Maximum likelihood phylogenies using a wide sampling of plastid and bacterial homologs (see Materials and Methods) also excluded a secondary bacterial origin for PsaA-1 as suggested previously (Mazor et al. 2012): although fast-evolving, both *C. velia* PsaA-1 and PsaA-2 were most closely related to the sister taxon *Vitrella* and other plastids.

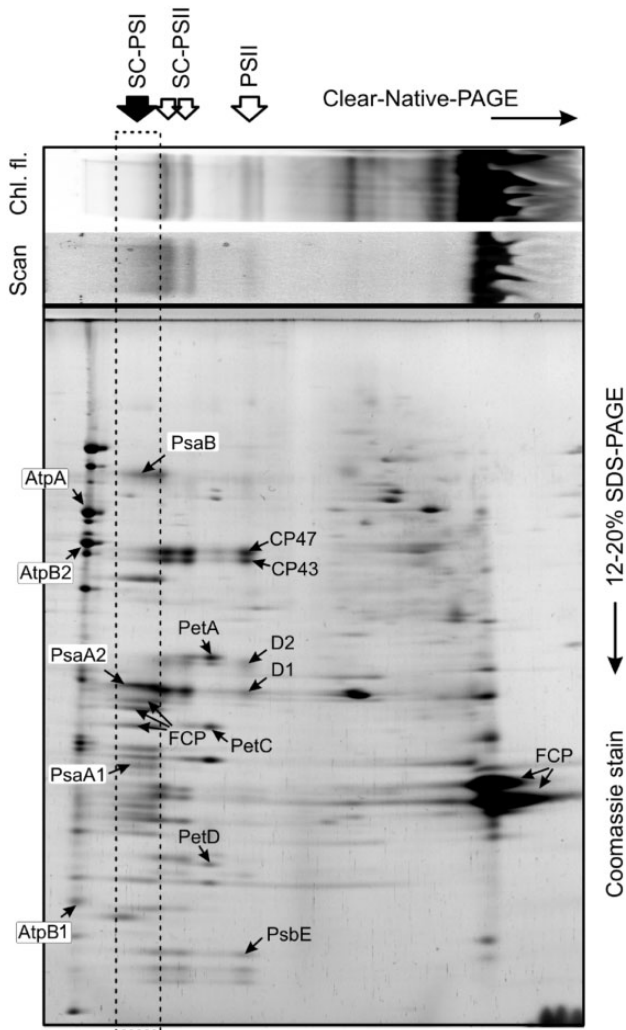


Fig. 3. The 2D electrophoresis of membrane protein complexes of *Chromera velia* and identification of individual spots. Membrane proteins were solubilized by dodecyl- β -maltoside and separated in the first dimension by Clear-Native electrophoresis (Clear-Native-PAGE). After the separation, the gel was scanned by LAS 4000 imager (Fuji, Japan) in chlorophyll fluorescence mode (Chl fl.) after excitation by blue LED light to distinguish the PSII and light-harvesting complexes. The protein complexes resolved in the first dimension were further separated in the second dimension by denaturing gel (SDS-PAGE) and stained by Coomassie blue. Protein spots were cut from the gel and analyzed by LC-MS/MS as described in Materials and Methods. Identified spots are highlighted and positions of protein complexes separated by Clear-Native electrophoresis are marked as follows: PSII: Photosystem II, SC-PSII: Supercomplexes of photosystem II with antenna, SC-PSI: Supercomplexes of photosystem I with antenna.

When compared with PsaA, the AtpB split is suggestive of a different, but equally interesting process. The region surrounding the split is conserved in plastid, mitochondrial, and bacterial homologs, but interrupted by a 24 amino acid (aa) insertion in *Vitrella*, *C. velia*'s closest photosynthetic relative (fig. 2C). A detailed sequence alignment of this region shows that the split in *C. velia* AtpB occurred within this shared insertion, suggesting that the ancestral acquisition of this insertion might have provided an evolutionary opportunity for the split. A 31 aa long insertion at the same site is

also present in the AtpB of the related dinoflagellate *Amphidinium* (data not shown). Although unrelated in sequence, the notorious divergence of dinoflagellate plastid proteins and their greater distance to *C. velia* and *Vitrella* could easily account for the insertion divergence pointing to a possibly even deeper origin.

Many Other Plastid Open Reading Frames are Extraordinary and Transcribed

PsaA and AtpB splits stand out as unprecedented cases but represent only a fraction of peculiarities in *C. velia* plastid open reading frames (ORFs). The genome contains many unusually modified ORFs, including several genes that are expected to be present in plastid genomes, but which are unusually large due to the presence of long extensions that bear no recognizable similarity to known genes. In three genes (*rps7*, 8, and 17), the ORF region has been extended by 126 to 273 amino acids toward the C-terminus effectively tripling them in size (supplementary fig. S2, Supplementary Material online). In four other genes (*rps3*, 4, 8, and 11), the region sharing homology with other plastid proteins is found at the end of an unusually large ORF (supplementary fig. S3, Supplementary Material online). The most obvious example of this is *Rps4*, which is encoded within a 1,998 aa long ORF, compared with 201 aa in the red alga *Porphyra purpurea*. In these cases, start codons may be located near the beginning of the homologous region, but it is still puzzling why the homologous region would be preceded by such a long stretch of sequence uninterrupted by stop codons. Canonical Shine-Dalgarno sequences are absent (the predicted 3'-end of the 16S rRNA is highly divergent in *C. velia*) and therefore cannot support start codon prediction. ORFs of two additional genes, *rpoC1* and *rpoC2*, contain long insertions (507 and 971 aa) in their variable regions (none of them appears to represent an intein; supplementary fig. S4, Supplementary Material online). Finally, a number of smaller changes are found in ORFs throughout the *C. velia* plastid genome. Accounting for extensions and indels longer than 20 aa, five other ORFs have a truncated N-terminus (*atpA*, *ccsA*, *petA*, *ycf3*, and *psaB*), one ORF has a significantly extended N-terminus (*rpl4*), two ORFs have a truncated C-terminus (*ccsA* and *rpoA*), five ORFs have an extended C-terminus (*atpA*, *atpB*, *atpH2*, *petA*, and *rps2*), and three ORFs contain intervening insertions (*rpl6*, *rpoB*, and *psaB*).

Altogether, ORFs of various functionally unrelated proteins contain unusual modifications. Many of the proteins are indispensable and exclusively plastid-encoded in algae and plants suggesting that they are unlikely to be in the process of degeneration, loss, or relocation to the nucleus in *C. velia*. Accordingly, none of these proteins can be identified in the available nuclear transcriptomes from *C. velia* (Woehle et al. 2011). To provide first insights into expression of the unusual proteins, we analyzed the plastid transcriptome using total and polyA RNA fraction sequence that we generated (polyU RNA sequence was not available for this analysis). Transcript mapping from the total RNA fraction (see Materials and Methods) revealed that all unusually long ORFs are covered by transcriptome reads roughly equally in their entirety

(supplementary figs. S2 and S3, Supplementary Material online). Although this approach cannot accurately pinpoint the position of start codons (many *rps* genes are expressed relatively little and intergenic regions are often transcribed), the consistent coverage by transcripts suggests that the ORFs may really have expanded in size at the protein level. Much of the long insertions in *rpo* genes is also equally represented in the transcriptome data; however, in this case a drop in coverage is found within each insertion creating a 200 bp gap (supplementary fig. S4, Supplementary Material online). This raises the possibility that RpoC1 and RpoC2 may be split much like PsaA and AtpB; however, both are in frame and low coverage, so more evidence is required to distinguish between the two alternatives.

Unusual changes to gene presence have also been noted: two genes are present in two (*atpH*) and three (*clpC*) full-length paralogs, despite that a single type is found in other plastid genomes. All three *clpC* paralogs are highly divergent in sequence from each other and *clpCs* in other plastids. They overlap only partially and the largest and most complete of the paralogs (*clpC3*) is an order of magnitude less expressed than the other two (supplementary fig. S5A, Supplementary Material online). Likewise, the two *atpH* paralogs are different in sequence (93% nucleotide similarity), length, and expression. *AtpH1* is both highly expressed and conserved, but the expression of the duplicated *atpH2* located on the TIRs is nearly 100-fold lower (supplementary fig. S5B, Supplementary Material online). The *atpH2* gene contains

an unusual C-terminal extension, which doubles it in size. A closer look at the surrounding sequence reveals that *atpH2* originated by a duplication event of the *atpH1* region (including *trnK*; discussed later). This, together with its low expression, suggests that *atpH2* is most likely a non-functional pseudogene. More generally, however, this example illustrates how duplication can drive gene paralogy, ORF expansion, and altered gene order; all features observed throughout the *C. velia* plastid genome.

Analysis of the total RNA and polyA fraction (fig. 4) transcription profiles revealed more unexpected features. Transcripts for all plastid genes were present in the total RNA fraction and consistently also found in the polyA fraction at two to three magnitudes lower abundance, probably due to a carryover of non-polyA transcripts (fig. 4). The *psbA* gene stood out in two ways, however. First, it was highly expressed, being represented at almost an order of magnitude higher levels than other protein-coding genes (and similar levels as the rRNA operon, fig. 4 and table 1). Second, the representation of *psbA* in the polyA fraction was about equal to the total RNA fraction, which would be the expected result for a polyadenylated transcript (fig. 4). Only two additional regions corresponding to *rps19* and a *psbB* fragment (part of the annotated *orf157*) were relatively overrepresented in the polyA fraction, but only *rps19* contained A-rich genomic sequence at the 3'-end that could explain the bias. Whether the *psbA* gene and *psbB* fragment are uniquely polyadenylated or a carryover into the polyA fraction occurred due to

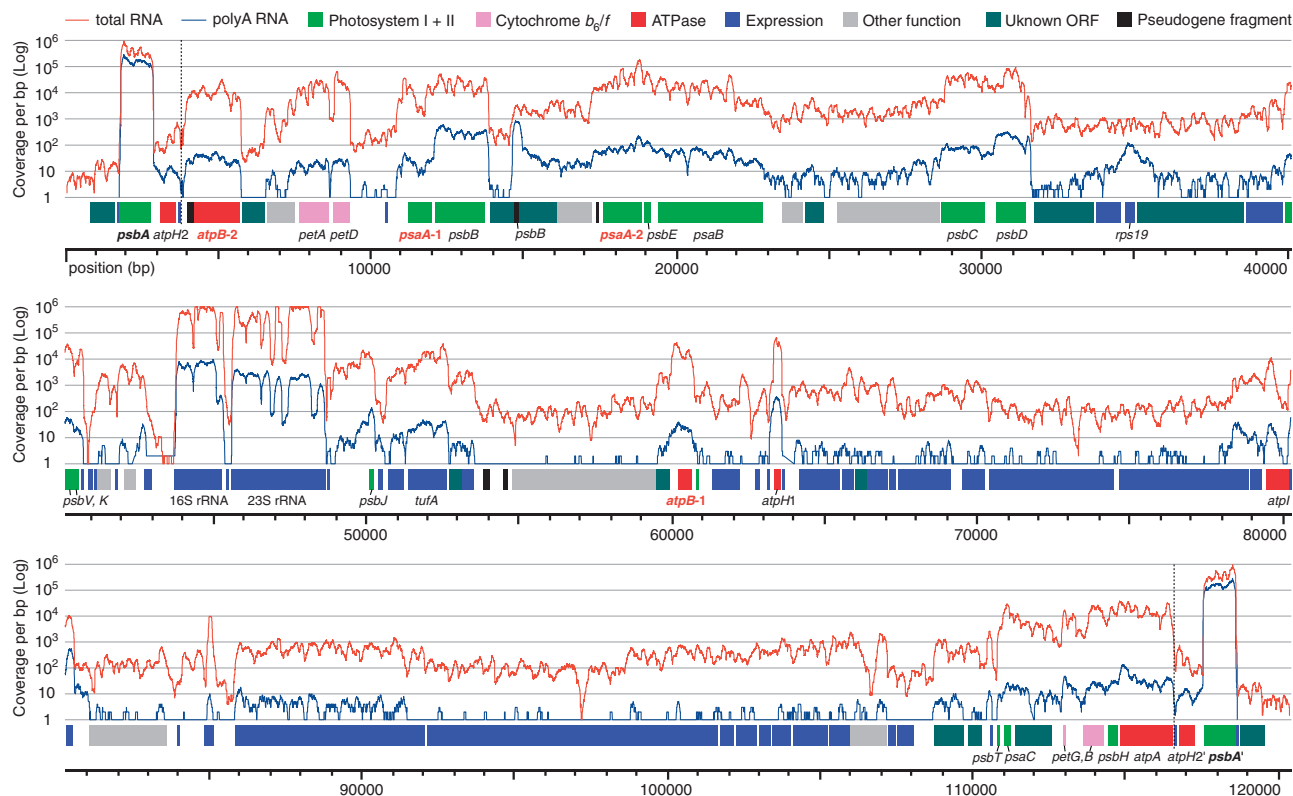


FIG. 4. Plastid total RNA and polyA RNA transcriptomic profiles. Coverage by total RNA (red) and polyA RNA (blue) is shown for the whole plastid genome (Log scale). Gene families are color-coded according to the key. The highly expressed *psbA* gene is highlighted in bold. The split *psaA* and *atpB* genes are in red. The boundaries of the TIRs are separated by dashed vertical lines.

another reason is currently not clear and awaits successful cloning of their 3' transcript ends. The transcriptomes also enabled us to analyze expression pattern among neighboring genes, which have been highly rearranged and strand-polarized in *C. velia* compared with other plastids. Canonical operons (*atpI/H/G/F/D/A*, *psaA/B*, *petB/D*, ribosomal protein supercluster, ribosomal RNA operon; e.g., Westhoff et al. 1983) and translationally coupled units (*atpB/E*; Gatenby et al. 1989) were also affected by rearrangements and either fragmented or internally reshuffled. Canonical promoters could not be identified. These characteristics indicate that transcription of many core plastid genes has been remodeled. Northern hybridization patterns in the *psaA-1* and *psaA-2* region already revealed that this is the case in several key proteins of the photosystems, which are expressed from novel multicistronic mRNAs through complex processing (fig. 1). Whole-genome transcriptional profiles (fig. 4) confirm this and suggest that polycistronic transcription is widespread in the genome (compare transcript coverage at intergenic spacers and the region downstream of the 16S rRNA gene; fig. 4). Although the primary transcript regions and processing patterns cannot be predicted accurately, the data show that novel polycistronic units most likely exist and often include functionally similar genes (compare distribution of genes for photosynthesis and protein expression in fig. 4).

Finally, we estimated and compared relative expression of all plastid genes separately, and in their functional groups based on the total RNA transcriptome (table 1 and supplementary table S3, Supplementary Material online). As expected, the rRNA genes were most highly expressed followed by genes of the four membrane complexes (PSI, PSII, cytochrome *b₆f*, and ATP synthase), and these also comprised all of the 22 most expressed protein-coding genes with the single exception of *tufA*. The least expressed were genes related to transcription and translation: RNA polymerase, tRNA genes, and ribosomal proteins (table 1). However, unknown ORFs and most intergenic regions were also expressed, including relatively highly expressed *orf389*, *orf201*, and intergenic regions downstream of *psbJ* and *atpB-1* (fig. 4). Additionally, we used the transcriptome to address the presence of RNA editing, which is known in the plastids of the related dinoflagellates (e.g., Dang and Green 2009), but has not been found in those of apicomplexans and *Vitrella*. The consensus of transcriptomic reads at each site was identical to the *C. velia* plastid genome sequence suggesting the absence of editing. Only four sites showed significant polymorphism (>10%) at RNA level (sites 44346 [51.5%], 46071 [23.66%], 46074 [39.35%], and 46574 [23.79%]), all of which were located within the rRNA operon and identical (99.8–100%) at the DNA level. Based on their location, we conclude that this is more likely due to reverse transcription errors of modified rRNA nucleosides, and not RNA editing.

A Linear-Mapping Plastid Genome in *C. velia*

One of the most significant features of the previously published plastid genome from *C. velia* is that it does not map as a circle as do all other plastid genomes completed to date. The gap in the sequence falls between the two copies of

the TIR containing *psbA* (Janouškovec et al. 2010). We attempted to close this gap using multiple approaches. We started by massively increasing the depth of sequence coverage. The genome was originally sequenced by 454 pyrosequencing to a 13-fold depth of coverage, so we used an independent approach and assembled the genome from paired-end Illumina sequence reads to an average depth of almost 600-fold. This approach extended the two TIRs by 300 bp on each side, which was verified by PCR (supplementary fig. S6, Supplementary Material online). The very end of each TIR was followed by a 15 bp sequence further followed by an extension into the complementary TIR at a very low depth of coverage (fig. 5). These extensions created an overlap between the ends; however, several lines of evidence suggested that this is not due to a circular chromosome, but rather a linear topology with structured ends. First, mapping the depth of coverage revealed a pattern expected for a linear molecule. The depth of coverage was generally consistent across the large single copy (LSC) region and most of the TIRs, but reduced linearly beginning at about 600 bp from the end, followed by an exponential reduction and partial recovery between 300 to 50 bp from the end, followed by a terminal drop (fig. 5A). The size and shape of the exponential reduction/recovery would be predicted by the mean DNA fragment size in the sequencing library (327 bp) and linear topology, as a consequence of fragmentation bias near the chromosome end. Therefore, both the overall decrease in coverage depth and the exponential decrease/recovery close to the ends support a linear chromosome conformation (if it were circular, the whole region should not differ from the rest of the genome). Second, if the genome was circular-mapping and the gap was hard to sequence, we would expect some paired ends to span the gap. However, when more than 650,000 paired ends are mapped to the genome, not a single paired end spanning the gap was identified (see Materials and Methods). Instead, both ends of the chromosome consisted exclusively of reverse-mapping reads (fig. 5A and B). Third, PCR experiments using six primers (all shown to successfully amplify products from one side of the gap) and all their nested combinations failed to fill the gap between the two TIRs (supplementary fig. S6, Supplementary Material online). Fourth, the size of the plastid genome estimated directly by pulsed-field gel electrophoresis (PFGE) and by *psbA* probe hybridization was consistent with abundant presence of linear monomers, 120 kb in size (supplementary fig. S7, Supplementary Material online, and Janouškovec et al. 2010). Subgenomic-sized material and unresolved DNA in the well were also abundantly represented, whereas putative linear dimers were rare and linear concatemers were not detected. The PFGE experiment was reproduced by using probes to three plastid genes encoded in the LSC region, *tufA*, *petA*, and *atpA* (see Materials and Methods), and consistently led to the same result, suggesting that linear monomers are an important constituent of plastid DNA in *C. velia*. Subgenomic-sized molecules could represent plastid DNA fragmented during PFGE preparation (note that intact *C. velia* cells were digested in agarose plugs, however), nucleus-encoded plastid DNA

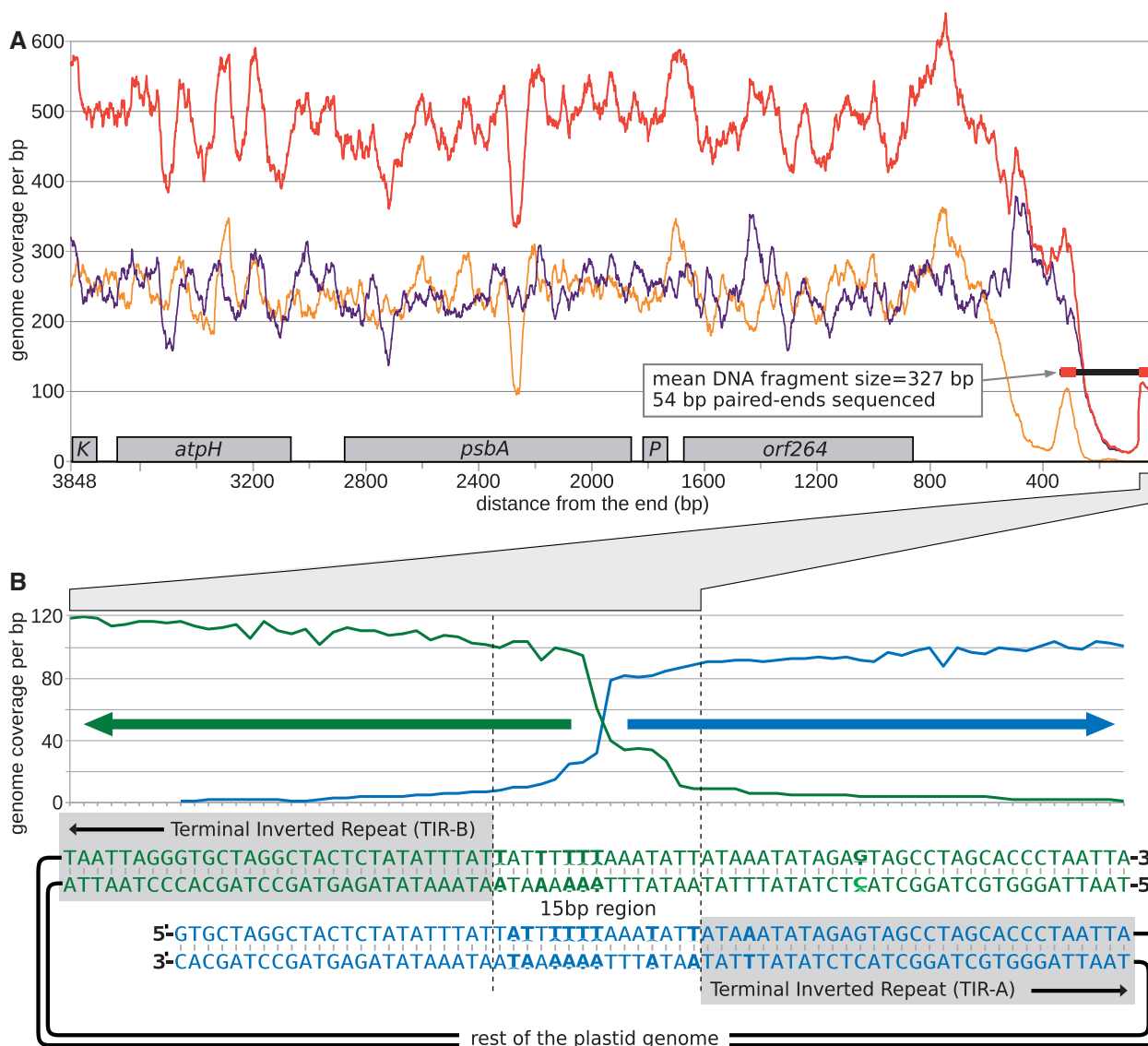


Fig. 5. Schematic of plastid chromosome ends. (A) Coverage depth (y axis) by forward-mapping (yellow), reverse-mapping (purple), and total (red) genomic reads is projected onto the TIR. Position of genes is shown by gray boxes at the bottom ($K = trnK$, $P = trnP$). Total coverage depth starts dropping gradually at about 800 bp from the chromosome end, and goes through a U-shaped minimum at about 150 bp from the end. The calculated mean size of the end-sequenced DNA fragments (horizontal black bar, red bits correspond to sequenced end pairs) and coverage by forward/reverse read pairs in this region suggest that the U-shaped minimum results from unequal DNA fragmentation near the chromosome end. A steep drop in total coverage depth occurs at the very end of the chromosome (B). Here, the TIRs on each of the chromosome ends (green and blue, respectively) diverge into a shared 15 bp region followed by a short sequence of the complementary TIR (DNA ends marked as 3' and 5'). The total depth of coverage by DNA reads (y axis) steeply decreases in the 15 bp region. The 15 bp region is also enriched in nucleotide discrepancies (sequence logos in bold). The last 130 bp at each chromosome end is exclusively assembled from reverse-oriented paired ends (horizontal colored arrows) and no paired-end spanning this region can be identified, suggesting that the genome cannot be genuinely circularized.

fragments, plastid DNA in the process of replication, or other forms of genuine plastid DNA (Ellis and Day 1986; Oldenburg and Bendich 2004; Scharff and Koop 2006). Incompletely digested cells of *C. velia* in the agarose plugs (see Materials and Methods) could be responsible for much of the signal in the well, although high-molecular-weight branched DNA forms could also be present and cannot be distinguished using the current approach (Bendich 1991; Bendich 2004). Altogether, because the plastid genome was not closed by deep sequencing using either 454 or Illumina, no paired-end linkage could be established, no linkage could be established by PCR, and

because the size of the plastid genome estimated by PFGE and Southern blot hybridizations was consistent with the existence of linear monomers, we conclude that the genome is principally linear in structure and circular molecules and linear concatemers are rare or absent.

If the genome is indeed linear, it will be important to know how the *C. velia* plastid DNA replication and copy number compares to the circular/concatemeric plastid DNA in apicomplexans (Williamson et al. 2001; Williamson et al. 2002) and other organisms. To provide a first glimpse into this, we identified a putative replication origin of the *C. velia*

plastid genome in silico using the cumulative GC-skew analysis. This region (68–69 kb from one end of the linear contig; [supplementary fig. S8A, Supplementary Material](#) online) is characterized by a minimum in cumulative GC-skew and loosely conserved tandem repeats (positions 68404–69029). In contrast, both ends of the chromosome are at a cumulative GC-skew maximum, suggesting that they most likely correspond to replication termini. Another feature commonly associated with origins of replication is the major shift in gene orientation, which is located approximately 18 kb away from the predicted replication origin in *C. velia* ([supplementary fig. S8B, Supplementary Material](#) online). The genomic region surrounding the two features is relatively overrepresented in the Illumina data, whereas both chromosome ends are relatively underrepresented (this holds after correction for base composition; [supplementary fig. S8C, Supplementary Material](#) online), which is consistent with the existence of replicating molecules in the Illumina library. Altogether, these three characteristics are consistent with linear-mapping topology and suggest that replication starts at about two-thirds of the way from one end of the molecule and proceeds bidirectionally toward the ends. The copy number for two *C. velia* plastid genes (*tufA* and *atpH*) was determined using dot blot hybridization to total genomic DNA and a synthetic construct (see Materials and Methods). The inferred copy number of both plastid genes was 9 times higher compared with a single-copy nuclear gene, topoisomerase II, and confirmed that genes encoded in the LSC region and TIR are equally represented (*atpH* is present in three closely related paralogs, all of which hybridized to the construct) ([supplementary fig. S9, Supplementary Material](#) online).

Discussion

Significance of Split Proteins for Photosynthesis and ATP Generation

Both PsaA and AtpB have never been observed to be fragmented like those of *C. velia*. Although the *psaA* gene is split in *Chlamydomonas reinhardtii*, RNA trans-splicing produces a full-length transcript, which is translated to a full-length protein (Merendino et al. 2006). The structure of the PSI core is highly conserved in all known oxygenic phototrophs (Nelson and Yocum 2006; Busch and Hippler 2011) and it is formed by a heterodimer of structurally similar PsaA and PsaB proteins, which bind a remarkably high number of cofactors: about 100 chlorophylls, 14 carotenoids, and 2 phylloquinones (Amunts et al. 2010). The algal PSI is expected to be structurally similar to the plant PSI including several Lhca antenna proteins bound in a half-circle around the PSI ([fig. 6A](#)).

PsaA in *C. velia* is split between domains 4 and 5 ([figs. 1 and 6A](#)). This suggests that the split was not simply a reversal of the proposed ancient formation of *psaA* by the gene fusion of a *psbB/psbC*-like antenna component and a *psbA/psbD*-like core of the reaction centre (domains 1–6 and 7–11, respectively, in [fig. 1; Schubert et al. 1998](#)). The position of the split and the faster evolutionary rate of PsaA-1 (peripheral fragment) can be reconciled with the structure of the PSI ([fig. 6A](#)

and B). Indeed, the presence of a supercomplex of PSI and antenna proteins in *C. velia* is obvious from the 2D electrophoresis ([fig. 3](#)). Apart from the structure of PSI itself, the process of the PSI assembly seems to be highly conserved through evolution from cyanobacteria to higher plant chloroplasts including assistance of the same auxiliary factors such as Ycf3 and Ycf4 (Boudreau et al. 1997; Ruf et al. 1997). Although many individual steps in the PSI biogenesis remain unknown, this process had to be remodeled in *C. velia* to assemble three proteins instead of two into the functional PSI core complex. Particularly intriguing is the binding of chlorophyll cofactors into the split PsaA. Both in vivo and in vitro studies suggest that chlorophyll has to be inserted into core subunits of PSI co-translationally, probably as a prerequisite for correct protein folding (Kim et al. 1994; Eichacker et al. 1996). The putative interface between PsaA-1 and PsaA-2 is rich in chlorophyll molecules ([fig. 6B](#)) and, according to available crystal structures, these chlorophylls are coordinated by both parts of split PsaA. It is not clear how *C. velia* inserts these chlorophylls into PSI and how stability and correct folding of the nascent PsaA-1/2 is achieved. Perhaps, both PsaA fragments are assembled together co-translationally, and this is synchronized with or even assisted by chlorophyll loading (which could also help to coordinate the orientation of the two fragments). In any case, the PSI core biogenesis in *C. velia* could involve additional synchronizing assembly step(s) and the recruitment of new, nuclear-encoded auxiliary factors. Interestingly, the second protein of the PSI antenna core, PsaB, mirrors some of the PsaA structure at functionally analogous positions: although not split, PsaB also contains a variable loop between the fourth and fifth trans-membrane helices and a highly divergent N-terminus. Whether this plays a compensatory role directly related to the splitting of PsaA is not clear, but it is an interesting possibility that would require direct biochemical testing.

Similar to the PsaA protein, any split of the AtpB protein would seem improbable due to its critical function and conserved structure. Even though the proposed AtpB-1 part of the β -subunit appears to be relatively far from the catalytic site ([fig. 6C](#)), it is known that tilting of the β -subunits including the top β -sheet crown is critical for the catalytic cycle. The movement of the upper part of the β -subunit is subtle, but if it is restricted by inhibitor tentoxin, then the cyclic interconversion of nucleotide binding sites is blocked (Groth 2002). Tentoxin binds close to the place where the AtpB protein is split (Groth 2002). Correct reassembly of AtpB-1 and AtpB-2 proteins is therefore likely to be highly constrained to avoid any restrictions of AtpB-2 movement. On the other hand, it is also possible that the fragmented AtpB-2 is more flexible and perhaps less sensitive to some natural inhibitors. The ATP synthase was also noteworthy in that it migrated at the top of the native protein gel. This has never been observed in cyanobacteria (Herranen et al. 2004) or higher plants (Järvi et al. 2011), and indicates that ATP synthase might be integrated into a very stable megadalton supercomplex in the plastid of *C. velia*.

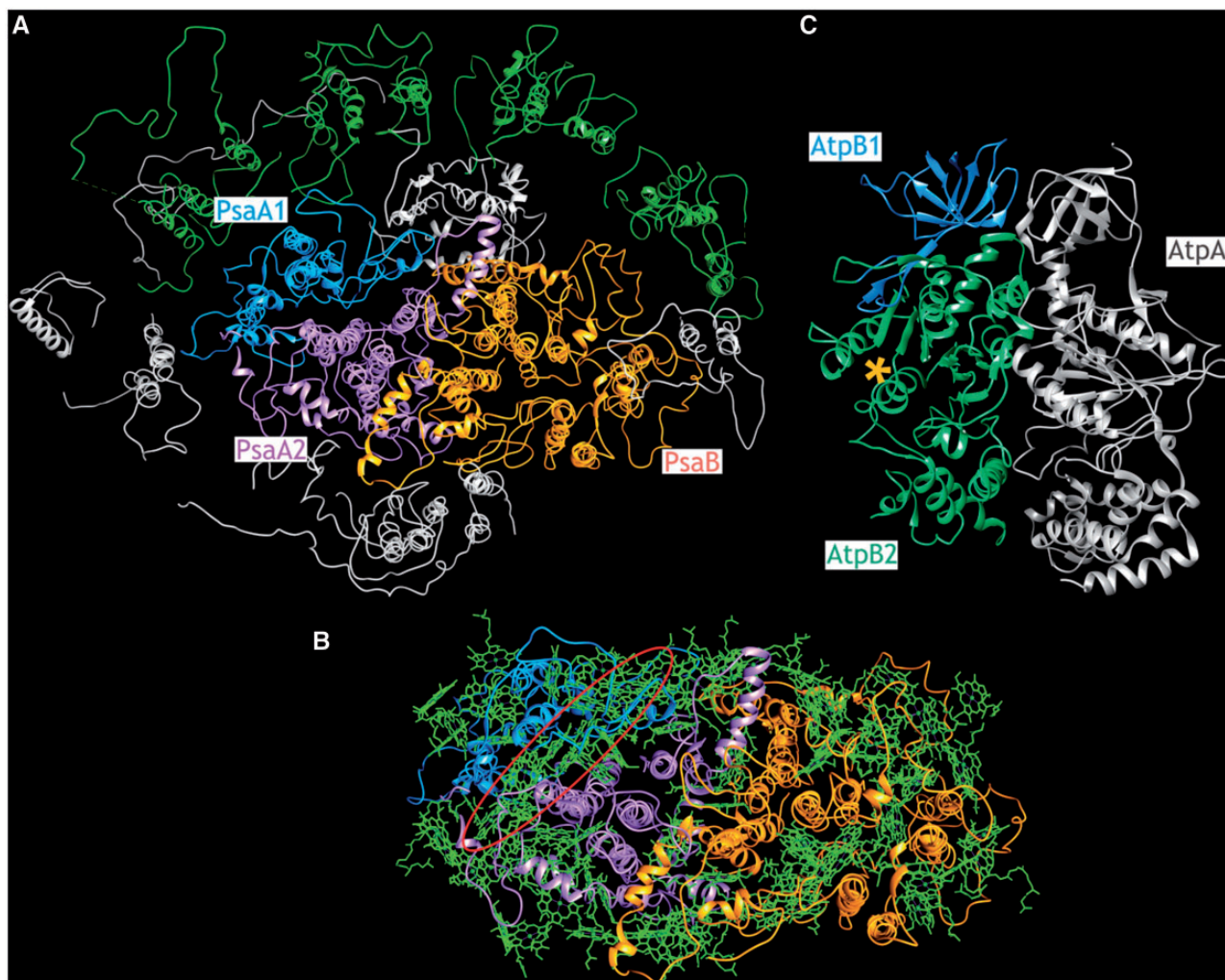


Fig. 6. A putative position of the PsaA proteins in PSI and the AtpB proteins in ATP synthase of *Chromera velia* as approximated from protein alignments and available crystal structures of plant counterparts. (A) A stromal view on the pea PSI-LHC complex (PDB ID code 2WSC; Amunts et al. 2009) showing a putative position of PsaA-1 and PsaA-2 in the PSI complex. Lhca antenna proteins are shown in green; stromal subunits PsaC, PsaD, and PsaE were removed for clarity. (B) A detail of the same structure showing arrangement of chlorophyll molecules bound to the PSI core. Red circle marks chlorophylls expected to be bound at an interface between PsaA-1 and PsaA-2 proteins in *C. velia* (see discussion for details). (C) AtpB-1 and AtpB-2 proteins fitted into structure of the spinach F_1 -ATPase (PDB ID code 1KMH). Catalytic site is indicated by an orange asterisk.

Highly Divergent Characteristics of Gene and Chromosomal Structure

A number of highly modified ORFs are found in the *C. velia* plastid genome and distributed without any obvious pattern. Long extensions or insertions in plastid proteins are uncommon in most plastids including those in other alveolates. Some have been identified in green algae (e.g., de Cambiaire et al. 2006), but never in the extent or number reported here. Many of the *C. velia* predicted proteins that contain extensions function in the small subunit of the ribosome. If the extensions are really present in the final functional proteins, this has implications for plastid ribosome structure. Alternatively, transcripts of the *rps* ORFs and other unusual ORFs could be modified so that only the homologous region is translated. This process may be related to transcript oligouridylation, but as yet we have no evidence to support this. OligoU tailing is another modification of general interest (Wang and Morse 2006) and its significance and distribution

in *C. velia* plastid transcripts remain unknown. OligoU tails in some *C. velia* transcripts are found in mature mRNAs that are derived from polycistronic primary transcripts (fig. 1). This suggests a possible role in transcript processing, perhaps similar to that observed in dinoflagellate plastids (Nelson et al. 2007; Dang and Green 2009; Barbrook et al. 2012). If confirmed, the ubiquitous presence of polycistronic transcription would imply that oligoU tailing is widespread in the *C. velia* plastid and tightly intertwined with expression of many core plastid genes.

No linear-mapping plastid genome has been documented to date, although there is a longstanding debate about whether circular-mapping plastid genomes might represent physically linear molecules (Bendich 2004). At a sufficient depth of coverage, the two ends of the *C. velia* plastid genome can be (barely) overlapped in sequence, but multiple lines of evidence suggest the genome is actually linear. The PFGE data support existence of linear monomers and rare

dimers (which could arise by TIR-mediated recombination between two monomers), but is incongruent with a significant presence of linear concatemers. This leaves no direct comparisons possible with other plastid DNAs, including those in related apicomplexans, which comprise various mixtures of circular molecules, linear concatemers, and high-molecular-weight material (Lilly et al. 2001; Williamson et al. 2002; Bendich 2004; Day and Madesis 2007). Presence of TIRs in the *C. velia* plastid genome is a common characteristic of linear genomes (e.g., in apicomplexan mitochondria; Kairo et al. 1994; Hikosaka et al. 2010). The physical structure of the chromosome ends remains unknown, but given the sequence one can speculate based on structures observed in other linear genomes. These include single-stranded loops (possibly followed by a nick) or single-stranded overhangs in the 15 bp regions (reviewed in Nosek et al. 2004), or diverse associations with end-specific proteins (e.g., Rekosh et al. 1977; Tomáška et al. 1997). Gradually decreasing depth of coverage near the chromosome end may also suggest that the whole terminal 600 bp region, not just its very end, is protected, possibly by a t-loop (Tomáška et al. 2002). No repeated sequence can be found close to the ends, however, so determining which of these structures, if any, most closely represents the physical state of the *C. velia* plastid chromosome will require direct testing. Altogether these data provide evidence for the first linear-mapping plastid genome in *C. velia*, and suggests that a similar topology could exist in other plastid genomes, particularly those that do not presently map as a circle (Gabrielsen et al. 2011).

The change in the plastid chromosome topology has important implications on the process of DNA replication and overcoming the end-replication problem. In the apicomplexan and other plastids, several types of replication origins have been identified and linked to the D-loop, rolling circle, and recombination-mediated replication strategies. The most common type of replication origin is associated with bidirectional D-loop replication and located inside the duplicated rRNA inverted repeat (Kolodner and Tewari 1975; Williamson et al. 2002; Krishnan and Rao 2009). In contrast, the *C. velia* plastid genome lacks both the duplicated rRNA unit and associated replication origin, and is probably replicated bidirectionally from the predicted putative replication origin toward the chromosome termini, which is a unique situation among all plastid genomes. The estimated plastid gene copy number ($9\times$ that of a nuclear marker) is also unusually low compared with most photosynthetic plastids ($\sim 50\text{--}100$ copies; Day and Madesis 2007), and is more similar to the gene copy number in the non-photosynthetic plastids of apicomplexans (~ 25 copies; Matsuzaki et al. 2001) or plastid minicircles during exponential growth in dinoflagellates (2–4 copies; Koumandou and Howe 2007).

Searching for Forces Driving Structural Complexity

The *C. velia* plastid genome is unique in a number of ways. Here, we have examined several unusual characteristics of its organization and expression, all of which raises the

question, why is this genome home to so many oddities? One property that might explain several of these characteristics concurrently is a high level of intragenomic duplication. The *C. velia* plastid genome has been extensively reshuffled and in order to understand the underlying forces we searched for palindromes, short repeats, and long repeats. Palindromes and short repeats were comparatively rare; however, the searches identified at least 46 pairwise matches between longer genomic sequences (>50 bp) at 65–100% similarity (fig. 7). Most of the duplicates are divergent and low copy number (2–3), and apart from the TIRs they include many intergenic regions, duplicated *atpH* and *clpC* genes, and duplicated fragments of otherwise complete genes (*psaA*, *psaB*, *psbB*, *rpl3*, and *tufA*; fig. 7). The region containing most repeated sequence is found around the TIR boundary (fig. 8). Multiple parts of this region, including several gene fragments, three *atpH* paralogs, and six *trnK* paralogs comprising both complete and fragmentary variants are scattered in several places in the genome (fig. 8). Long repeats are rare in most plastids, suggesting that duplication is an important force in shaping the *C. velia* plastid genome. Duplication could explain occurrence of paralogs, small gene fragments, extensive gene re-shuffling, and re-structuring of operon units through movement of promoters and intergenic elements. Similar processes could account for the addition of extensions and insertions to genes. The splitting of *psaA* and *atpB* could likewise be seen as a process involving duplication or partial duplication. For example, the *PsaA* split could have proceeded through an intermediate, in which the

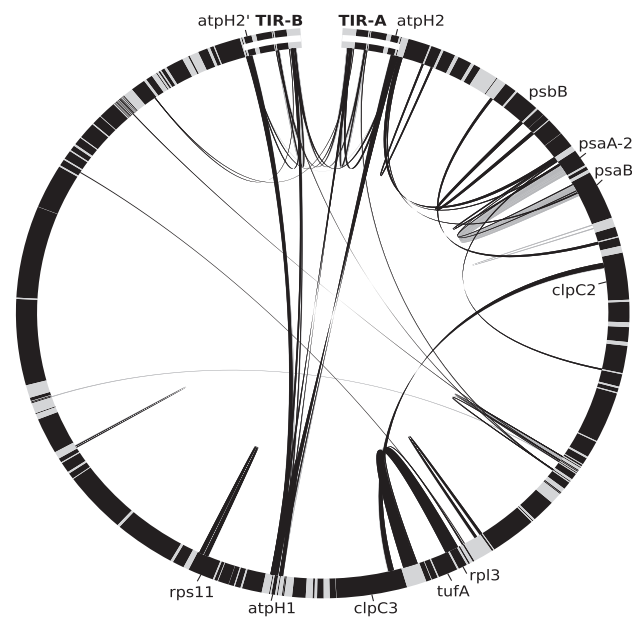


FIG. 7. Large repeats in the *Chromera velia* plastid genome. The linear genome is drawn as an incomplete circle with genes in black, intergenic in light gray, and two TIRs (white lines) at chromosome ends (15 bp regions at the termini are not visible here). Links connect homologous regions of 50 bp or more identified by BLAST (dark gray) and additional matches identified by Pipmaker (medium gray). Homology between the TIRs is not shown for clarity. Names of genes most affected by duplication events are indicated.

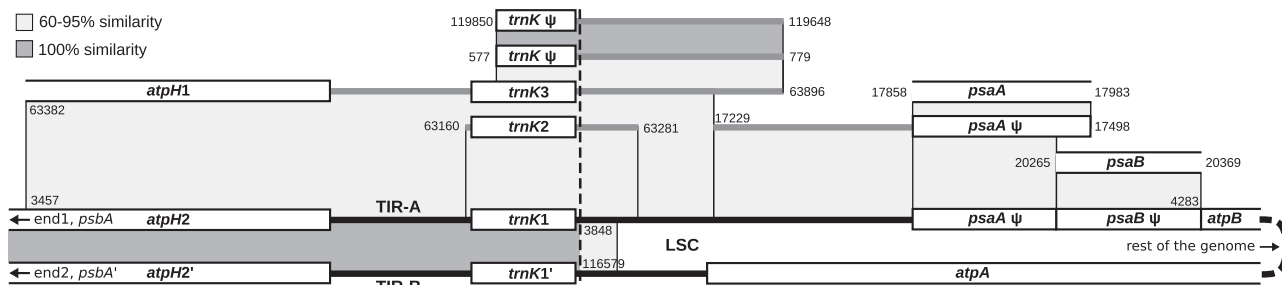


Fig. 8. Intrachromosomal duplication and recombination hotspot around the TIR boundary (vertical dashed line). The plastid genome is shown by thick black line at the bottom with TIRs (TIR-A and TIR-B) folded onto themselves to the left and the LSC region forming a loop to the right. Other parts of the genome with homology to the TIR boundary region are shown by thick gray lines; numbers indicate positions. Genes and pseudogenes are shown by boxes. Level of sequence similarity is distinguished according to the key.

canonical and split Psas coexisted. In this scenario, each of the two complexes could have been regulated independently and potentially even have different functions much alike the cyanobacterial monomeric and trimeric PSI (Majeed et al. 2012).

Duplicated sequences in *C. velia* plastid are low copy number, long, and divergent from each other. They are dissimilar from short dispersed repeats found in some algal plastids (e.g., in *Chlamydomonas*; Maul et al. 2002) and longer repeats found in angiosperm plastids (e.g. Guisinger et al. 2011), all of which are conserved in sequence and comparatively high copy number. It remains unclear how duplication is mediated in *C. velia*. Few duplicates are in tandem so the duplication process is not likely to be related to DNA replication and is more likely related to recombination. A functional DNA recombination machinery has been documented in several land plant and algal plastids (Palmer 1983; Boynton et al. 1988; Haberle et al. 2008), where it primarily acts in DNA repair and replication. Unwanted genome reorganization is known to be actively prevented, which explains why most plastids have maintained a conserved genomic architecture (reviewed in Maréchal and Brisson 2010). It is possible that mechanisms preventing unwanted recombination or, alternatively, those allowing for recombination-mediated repair were loosened or lost in the *C. velia* plastid, which led to propagation of duplicates and rearrangements. The apparent linearization of the chromosome could also stem from a recombination-mediated rearrangement involving homologous TIRs and 15 bp repeats now located at the termini. Interestingly, although sequence shuffling has been extensive in the *C. velia* plastid genome, it has not been completely random. Most genes have been reorganized in large clusters with a strongly pronounced strand polarity (supplementary fig. S8B, Supplementary Material online). More importantly, functionally related genes often cluster together and are most likely transcribed polycistronically (fig. 4), so even with high levels of rearrangement a functionally reorganized genomic architecture can result from selection.

Intragenomic duplication may be the cause of most peculiarities in the *C. velia* plastid genome, but not all of them. Features such as transcript oligoU tailing and noncanonical genetic code (Moore et al. 2008; Janouškovec et al. 2010) may

have different causes including increased mutation rate, small population size, and a short replication cycle. Moreover, early evolutionary acquisition and long-term combined effect of some these forces could have significantly contributed to the genome remodeling. For example, all alveolate plastids (*C. velia*, apicomplexans, *Vitrella*, and dinoflagellates) have a reduced gene complement, somewhat modified gene order, and comparatively fast rate of protein evolution (Janouškovec et al. 2010). Oligouridylation of plastid transcripts is also found in dinoflagellates and may significantly predate *C. velia*, although it seems to be missing in apicomplexans (Janouškovec et al. 2010; J.J. unpublished data). The AtpB insertion present in dinoflagellates and *Vitrella* at a homologous position to the split in *C. velia* could be viewed as an ancestral acquisition that may have individualized the two parts of the protein preparing ground for the split. Similarly, recombination has been very active in the dinoflagellate plastids and possibly even led to a massive fragmentation of their genome to small mini-circles (Zhang et al. 1999; Zhang et al. 2001), so it might be tempting to speculate that the core cause of many of these conditions traces back to an ancient ancestor. Distinguishing between ancient and independent gains is nevertheless difficult. The plastid genomes of apicomplexans and *Vitrella* are generally not that unusual in structure as *C. velia* and dinoflagellates, so it is more accurate to propose that all alveolate plastids were ancestrally somewhat divergent, but evolved in different directions.

The fact that in a single organism two conservative photosynthesis proteins are split is astonishing given the high efficiency of *C. velia* photosynthesis (Quigg et al. 2012). The mechanism behind a particular split can be relatively simple, but it is more difficult to see how each of the PsaA and AtpB fragments became integrated into a functional multiprotein complex. For example, both PsaA fragments had to coevolve with mechanisms allowing co-translational insertion of chlorophylls, and simultaneously acquire/remodel interactions with numerous cofactors that mediate their assembly into a fully functional PSI complex. Many other structures in the *C. velia* plastid appear similarly complicated. Both the ribosome and RNA polymerase complex comprise a number of highly modified components including proteins with hundreds of amino acid long extensions and insertions. Explaining the appearance of highly modified structures

is more difficult than their components individually, because many parts of these systems are mutually constrained. Likewise, molecular processes such as oligoU tailing are difficult to justify in adaptive terms. Considering the complexity of similar unnecessary processes in other organelles, such as RNA editing or intron splicing (Gray et al. 2010), it is attractive to hypothesize that complicated molecular machineries have evolved in the *C. velia* plastid that serve no general advantage.

Materials and Methods

DNA Extraction, Sequencing, Annotation, and Fragmented Gene Analysis

Pelleted cells of *C. velia* were ground in liquid nitrogen using mortar and pestle and the resulting slurry was incubated in CTAB buffer (2% w/v cetyltrimethyl ammonium bromide; 1.42 M NaCl; 20 mM EDTA; 100 mM Tris HCl, pH 8.0; 2% w/v polyvinylpyrrolidone 0.5% β -mercaptoethanol; 1 mg/ml RNase A) at 65 °C for 20 min. After two extractions with phenol/chloroform and one with chloroform only, DNA was precipitated with isopropanol and washed with ethanol. Pellet was dried at room temperature and resuspended in TE buffer. Extracted DNA was separated by CsCl-Hoechst gradient ultracentrifugation and AT-enriched fractions were tested for the presence of plastid DNA using the *psbA* probe. Plastid-enriched DNA fractions were sequenced using Illumina 54 bp paired-end reads technology (a total of 9,591,179 read pairs were obtained) and deposited in GenBank Sequence Read Archive (Bioproject PRJNA193178). De novo sequence assembly using MIRA3 extended the previous plastid contig (NC_014340.1) at both ends to the final length of 120,426 nucleotides at 572 \times average depth of coverage. Two errors at homopolymeric regions were corrected, which led to the merging of *rps7* with *orf142* and *rpl4* with *orf128*. The gene for 5S ribosomal RNA was identified upstream of 23S rRNA, and its fold verified using Mfold (<http://mfold.rna.albany.edu/?q=mfold>, last accessed May 25, 2013). Proteins were re-annotated by comparison with plastid homologs from an NTG start codon with the exception of 10 proteins that were more consistent with an AT[A,C,T] start codon. Six of the proteins had no alternative NTG start (*atpA*, *rpl31*, *rps7*, *rps12*, *rps14*, *ycf3*). Unknown ORFs and genes with long N-terminal extensions were annotated from the first NTG start codon. The extended plastid genome sequence and new annotations were deposited in an updated *C. velia* plastid genome entry (NC_014340.2). PsaA trans-membrane domains were predicted using TMHMM 2.0 (<http://www.cbs.dtu.dk/services/TMHMM/>, last accessed May 25, 2013) and by comparison to PsaA of *Synechococcus elongatus*. The corrected genetic distances for PsaA-1 and PsaA-2 were calculated in Tree-Puzzle 5.2 (Schmidt et al. 2002) using a data set of 40 representative plastid PsaA homologs and the following parameters: Likelihood mapping, Slow (exact) parameter estimates, WAG model with four gamma categories, estimated alpha parameter, and estimated aa frequencies. PsaA-1/2 phylogenies were

computed using a broader data set in RAxML using -m PROTGAMMALGF -f a -# 100. PsaA-1/2 and AtpB data sets were aligned using -localpair option in MAFFT.

RNA Extraction, RACE, and Northern Blot Hybridization

Total RNA was isolated from ~0.2 g of *C. velia* cells ruptured by repeated freezing and thawing, followed by grinding with a pestle in liquid nitrogen, by the addition of 5 ml TRI reagent, followed by manufacturer's instructions (Sigma). Total RNA was ligated with 5' adapter (5' RACE) or self-ligated with T4 RNA ligase (circular RACE), and RT-PCR was carried out with either random or specific primers, or with polyT primers (3' RACE). Sequences of circularized transcripts were deposited under GenBank Nucleotide accessions KC734564–KC734569. For Northern blot analysis, ~10 μ g per lane of total RNA was separated in a 1% formaldehyde agarose gel in 1 \times MOPS buffer, blotted, and UV cross-linked as described elsewhere (Vondrušková et al. 2005). PCR-amplified DNA fragments of selected genes (for primers see [supplementary table S4, Supplementary Material](#) online) were labeled by random priming with [α ³²P]-dATP and used as probes for hybridization at 55 °C. After washing, the results were visualized on Typhoon Imaging System (GE Healthcare).

Preparations of Cell Membranes and Two Dimensional Electrophoresis

Cells of *C. velia* (optical density at 750 nm = ~0.5) were washed and resuspended in 1 ml of the working buffer containing 25 mM MES/NaOH, pH 6.5, 5 mM CaCl₂, 10 mM MgCl₂, and 20% glycerol. The resuspended cells were mixed with 0.5 ml of glass beads (0.1 mm diameter) in 2 ml eppendorf tube and broken using Mini-BeadBeater (BioSpec; eight shaking cycles, 10 s each with 2-min breaks for cooling the suspension on ice). Membranes were separated from the cell extract by centrifugation (40,000 \times g, 20 min). The isolated membranes were resuspended in the working buffer and solubilized by gentle shaking with 1% dodecyl- β -maltoside at 10 °C for 1 h. Insoluble parts were removed by centrifugation (65,000 \times g, 20 min). Analysis of native membrane complexes was performed using Clear-Native electrophoresis as described in Wittig and Schagger (2008). Individual proteins in membrane complexes were resolved in the second dimension by SDS-PAGE in a 12–20% linear gradient polyacrylamide gel containing 7 M urea (Sobotka et al. 2008).

Protein Identification by LC-MS/MS Analysis

Gel slices were placed in 200 μ l of 40% acetonitrile, 200 mM ammonium bicarbonate, and incubated at 37 °C for 30 min. The solution was then discarded, the procedure was repeated one time, and the gel was finally dried in a vacuum centrifuge. Twenty microliters of 40 mM ammonium bicarbonate containing 0.4 μ g trypsin (proteomics grade, Sigma) was added to the tube, incubated at 4 °C for 45 min, and then dried in a vacuum centrifuge. To digest proteins, 20 μ l of 9%

acetonitrile in 40 mM ammonium bicarbonate was added to the gel and incubated at 37 °C overnight. Peptides were purified using ZipTip C18 pipette tips (Millipore Corporation) according to manufacturer's protocol. MS analysis was performed on NanoAcquity UPLC (Waters) on-line coupled to the ESI Q-ToF Premier mass spectrometer (Waters). One microliter of the sample was diluted in 3% acetonitril/0.1% formic acid and tryptic peptides were separated using the Symmetry C18 Trapping column (180 µm i.d. × 20 mm length, particle size 5 µm, reverse phase, Waters) with a flow rate of 15 µl/min for 1 min. It was followed by a reverse-phase UHPLC using the BEH300 C18 analytical column (75 µm i.d. × 150 mm length, particle size 1.7 µm, reverse phase, Waters). Linear gradient elution was from 97% solvent A (0.1% formic acid) to 40% solvent B (0.1% formic acid in acetonitrile) at a flow rate of 0.4 µl/min. Eluted peptides flowed directly into the ESI source. Raw data were acquired in data-independent MS^e identity mode (Waters). Precursor ion spectra were acquired with collision energy 5 V and fragment ion spectra with a collision energy 20–35 V ramp in alternating 1 s scans. For the second analysis, data-dependent analysis mode was used; peptide spectra were acquired with collision energy 5 V, and peptides with charge states of +2, +3, and +4 were selected for MS/MS analysis. Fragment spectra were collected with a collision energy 20–40 V ramp. In both modes, acquired spectra were submitted for database searching using the PLGS2.3 software (Waters) against the predicted proteins coded by the plastid genome of *C. velia* and against the available EST sequences (www.ncbi.nlm.nih.gov, last accessed May 25, 2013). Acetyl N-terminal, deamidation N and Q, carbamidomethyl C, and oxidation M were set as variable modifications. Identification of three consecutive y- or b-ions was required for a positive peptide match and a minimum of three peptide matches were required for a positive protein identification.

Transcriptome Analysis

Total RNA and polyA RNA fraction were sequenced using Illumina paired-end read technology. Read coverage depth was averaged across the two TIRs. Coverage values for all sites were then exported and plotted in a spread sheet editor. Incorrect read mapping to duplicated genes (*atpH* and *clpC*) and repeated regions was ruled out based on match length or sequence divergence (all matches were 96.6% similar or lower). Presence of RNA editing was assessed by comparing relative representation of high-quality nucleotides (Phred score 30 or higher) at each site in between transcriptomic and genomic reads mapped on the plastid contig.

DNA Read Mapping, Chromosome Ends Analysis, and Repeat Analysis

Illumina paired-end DNA reads were separately mapped on the linear and artificially circularized plastid genome sequence using Consed 2.2 and Bowtie 2.0 under default settings (667,715 read pairs mapped). Read coverage depth was averaged across the two TIRs and incorrect read mapping to repeats was ruled out as above. Coverage depth

by forward-oriented (i.e., oriented outside of the chromosome) and reverse-oriented reads was calculated using Bedtools 2.17. No forward-oriented reads were found within the last 130 bp of the chromosome ends (all reads in this region were reverse-oriented). Only 23 forward-oriented reads were found within the last 250 bp of the chromosome ends, all of which had a reverse-oriented pair mapping close to the chromosome end except 6 reads whose pairs did not map to the plastid genome sequence or each other. In order to estimate the mean DNA fragment size, full-length read pairs (54 bp each) were mapped on the plastid contig using Bowtie 2.0, and sorted and analyzed using Picard Tools SortSam.jar and CollectInsertSizeMetrics.jar utilities. Discrepant bases in figure 5B were visualized using WebLogo 3 (<http://weblogo.threeplosone.com/create.cgi>, last accessed May 25, 2013) using “Base probabilities” as units and “No adjustment for base composition” setting. PCR on genomic DNA was done at the following conditions: annealing at 55 °C, 30 s to 4 min elongation times, and 35 cycles. All six primers used in bridging the gap between the two contig ends were confirmed to give functional products with a different primer pair under the same conditions (supplementary fig. S6C and D, Supplementary Material online). Palindromes and repeats were searched using EMBOSS 6.3.1 repeat identification tools at Pasteur Mobyly website (<http://mobyly.pasteur.fr/>, last accessed May 25, 2013), Pipmaker (<http://pipmaker.bx.psu.edu/pipmaker/>, last accessed May 25, 2013), and pairwise BlastN searches (length >50 nucleotides, e-value <0.01, and sequence similarity 65–100%), all at default settings. Figure 7 was plotted using Circos.

PFGE and Southern Blot Hybridization

Chromera velia cells (10^7 – 10^8) were slowly pelleted, embedded in low-melting agarose plugs, and treated with 2% *N*-laurylsarcosine and 2 mg/ml proteinase K for 28 h at 56 °C. Thick cell walls in *C. velia* prevented efficient penetration of cell membranes and DNA release leaving between 10% and 30% of all cells undigested. The plugs were inserted into 1% agarose gel and DNA was resolved on CHEF-DR III PFGE (Bio-Rad) in 0.5× TBE at 14 °C and using two different settings: 1) $U = 6$ V/cm with 0.5–25 s pulses and 120° angle for 20 h and 2) $U = 6$ V/cm with 0.1–2 s pulses and 120° angle for 14 h. After treatment with 0.25 M HCl for 20 min, the gels were denatured, neutralized, and blotted to nylon membrane and UV cross-linked following standard protocols. DNA probes were labeled as described above. Southern blot analysis with *psbA*, *tufA*, *petA*, and *atpA* probes (see supplementary table S4, Supplementary Material online, for primers) was performed in NaPi solution (0.5 M Na₂HPO₄, pH 7.2, 1 mM EDTA, 7% SDS, 1% BSA) at 65 °C overnight, and the membranes were washed 20 min in 2× SSC, 0.1% SDS at room temperature and another 20 min in 0.2× SSC, 0.1% SDS at 65 °C, and visualized on Typhoon Imaging System (GE Healthcare).

Determining the Replication Origin and Plastid Gene Copy Number

The cumulative GC skew plot was drawn using the utility at http://gcat.davidson.edu/DGPB/gc_skew/gc_skew.html (last accessed May 25, 2013). Coverage depth by Illumina genomic reads was determined as above. Relative abundance of selected plastid and nuclear genes in *C. velia* were estimated as follows. A 519 bp-long fragment of nuclear topoisomerase II gene (a typical single-copy nuclear gene), and 337 bp-long and 327 bp-long fragments of chloroplast *tufA* and *atpH2* genes, respectively, were cloned in tandem into a single plasmid, using unique restriction sites in the primers (supplementary table S4, Supplementary Material online). The resulting construct was labeled p55+13. Separate serial dilutions of total DNA of *C. velia* digested with Dral and Sph1103I and the EcoRV-linearized p55+13 were spotted on a Biodyne membrane (Pall), cross-linked, and blotted as described above. Each gene fragment (Topo II, *tufA*, *atpH*) was labeled by [$\alpha^{32}\text{P}$]ATP, hybridized at 65 °C to one of three identical blots, and visualized as above. The *atpH2* probe was tested to hybridize efficiently to all three *atpH* paralogs (two of which are identical to the probe and the third is 93% identical). For this, genomic DNA digested with Dral and Sph1103I was resolved in a 0.75% agarose gel, blotted, and hybridized as above, and signals from *atpH1* and *atpH2*-specific fragments were compared.

Supplementary Material

Supplementary figures S1–S9 and tables S1–S4 are available at *Molecular Biology and Evolution* online (<http://www.mbe.oxfordjournals.org/>).

Acknowledgments

This work was supported by a grant from the Canadian Institutes of Health Research to P.J.K. (MOP-42517); by the Czech Science Foundation projects P506/12/1522 and P501/12/G055 to M.O.; by the Praemium Academiae award to J.L.; by Award IC/2010/09 by the King Abdullah University of Science and Technology (KAUST) to A.P., M.O., and J.L.; and by the project Algatech (CZ.1.05/2.1.00/03.0110) to R.S., J.K., and O.P.. P.J.K. and J.L. are Fellows of the Canadian Institute for Advanced Research. P.J.K. was supported by a Fellowship from the John Simon Guggenheim Foundation.

References

- Amunts A, Toporik H, Borovikova A, Nelson N. 2010. Structure determination and improved model of plant photosystem I. *J Biol Chem.* 285:3478–3486.
- Barbrook AC, Dorrell RG, Burrows J, Plenderleith LJ, Nisbet RER, Howe CJ. 2012. Polyuridylation and processing of transcripts from multiple gene minicircles in chloroplasts of the dinoflagellate *Amphidinium carterae*. *Plant Mol Biol.* 79:347–357.
- Bendich AJ. 1991. Moving pictures of DNA released upon lysis from bacteria, chloroplasts, and mitochondria. *Protoplasma* 160:121–130.
- Bendich AJ. 2004. Circular chloroplast chromosomes: the grand illusion. *Plant Cell* 16:1661–1666.
- Botté CY, Yamaryo-Botté Y, Janouškovec J, Rupasinghe T, Keeling PJ, Crellin P, Coppel RL, Maréchal E, McConville MJ, McFadden GI. 2011. Identification of plant-like galactolipids in *Chromera velia*, a photosynthetic relative of malaria parasites. *J Biol Chem.* 286:29893–29903.
- Boudreau E, Takahashi Y, Lemieux C, Turmel M, Rochaix J-D. 1997. The chloroplast *ycf3* and *ycf4* open reading frames of *Chlamydomonas reinhardtii* are required for the accumulation of the photosystem I complex. *EMBO J.* 16:6095–6104.
- Boynton JE, Gillham NW, Harris EH, et al. (11 co-authors). 1988. Chloroplast transformation in *Chlamydomonas* with high velocity microprojectiles. *Science* 240:1534–1538.
- Busch A, Hippler M. 2011. The structure and function of eukaryotic photosystem I. *Biochim Biophys Acta* 1807:864–877.
- Dang Y, Green BR. 2009. Substitutional editing of *Heterocapsa triquetra* chloroplast transcripts and a folding model for its divergent chloroplast 16S rRNA. *Gene* 442:73–80.
- Day A, Madesis P. 2007. DNA replication, recombination, and repair in plastids. In: Bock R, editor. *Cell and molecular biology of plastids*. Berlin: Springer. p. 65–119.
- de Cambiaire J-C, Otis C, Lemieux C, Turmel M. 2006. The complete chloroplast genome sequence of the chlorophycean green alga *Scenedesmus obliquus* reveals a compact gene organization and a biased distribution of genes on the two DNA strands. *BMC Evol Biol.* 6:37.
- Eichacker LA, Müller B, Helfrich M. 1996. Stabilization of the chlorophyll binding apoproteins, P700, CP47, CP43, D2, and D1, by synthesis of Zn-phytyl *a* in intact etioplasts from barley. *FEBS Lett.* 395:251–256.
- Ellis TH, Day A. 1986. A hairpin plastid genome in barley. *EMBO J.* 5:2769–2774.
- Gabrielsen TM, Minge MA, Espelund M, et al. (11 co-authors). 2011. Genome evolution of a tertiary dinoflagellate plastid. *PLoS One* 6:e19132.
- Gatenby A, Rothstein S, Nomura M. 1989. Translational coupling of the maize chloroplast *atpB* and *atpE* genes. *Proc Natl Acad Sci U S A.* 86:4066–4066.
- Gray MW, Lukeš J, Archibald JM, Keeling PJ, Doolittle WF. 2010. Irremediable complexity? *Science* 330:920–921.
- Green BR. 2003. The evolution of light-harvesting antennas. In: Green BR, Parson WW, editors. *Light-harvesting antennas in photosynthesis*. Netherlands: Kluwer Academic Publishers. p. 129–168.
- Groth G. 2002. Structure of spinach chloroplast F1-ATPase complexed with the phytopathogenic inhibitor tentoxin. *Proc Natl Acad Sci U S A.* 99:3464–3468.
- Guisinger MM, Kuehl JV, Boore JL, Jansen RK. 2011. Extreme reconfiguration of plastid genomes in the angiosperm family Geraniaceae: rearrangements, repeats, and codon usage. *Mol Biol Evol.* 28:583–600.
- Haberle RC, Fourcade HM, Boore JL, Jansen RK. 2008. Extensive rearrangements in the chloroplast genome of *Trachelium caeruleum* are associated with repeats and tRNA genes. *J Mol Evol.* 66:350–361.
- Herranen M, Battchikova N, Zhang P, Graf A, Sirpiö S, Paakkarinen V, Aro E-M. 2004. Towards functional proteomics of membrane protein complexes in *Synechocystis* sp. PCC 6803. *Plant Physiol.* 134:470–481.
- Hikosaka K, Watanabe Y-I, Tsuji N, et al. (12 co-authors). 2010. Divergence of the mitochondrial genome structure in the apicomplexan parasites, *Babesia* and *Theileria*. *Mol Biol Evol.* 27:1107–1116.
- Janouškovec J, Horák A, Barott KL, Rohwer FL, Keeling PJ. 2012. Global analysis of plastid diversity reveals apicomplexan-related lineages in coral reefs. *Curr Biol.* 22:R518–R519.
- Janouškovec J, Horák A, Obornik M, Lukeš J, Keeling PJ. 2010. A common red algal origin of the apicomplexan, dinoflagellate, and heterokont plastids. *Proc Natl Acad Sci U S A.* 107:10949–10954.
- Järvi S, Suorsa M, Paakkarinen V, Aro E. 2011. Optimized native gel systems for separation of thylakoid protein complexes: novel super- and mega-complexes. *Biochem J.* 439:207–214.
- Jordan P, Fromme P, Witt HT, Klukas O, Saenger W, Krauss N. 2001. Three-dimensional structure of cyanobacterial photosystem I at 2.5 Å resolution. *Nature* 411:909–917.
- Kairo A, Fairlamb AH, Gobright E, Nene V. 1994. A 7.1 kb linear DNA molecule of *Theileria parva* has scrambled rDNA sequences

- and open reading frames for mitochondrially encoded proteins. *EMBO J.* 13:898–905.
- Kim J, Eichacker LA, Rudiger W, Mullet JE. 1994. Chlorophyll regulates accumulation of the plastid-encoded chlorophyll proteins P700 and D1 by increasing apoprotein stability. *Plant Physiol.* 104:907–916.
- Kolodner RD, Tewari KK. 1975. Chloroplast DNA from higher plants replicates by both the Cairns and the rolling circle mechanism. *Nature* 256:708–711.
- Kořený L, Sobotka R, Janouškovec J, Keeling PJ, Oborník M. 2011. Tetrapyrrole synthesis of photosynthetic chromerids is likely homologous to the unusual pathway of apicomplexan parasites. *Plant Cell* 23:3454–3462.
- Koumandou VL, Howe CJ. 2007. The copy number of chloroplast gene minicircles changes dramatically with growth phase in the dinoflagellate *Amphidinium operculatum*. *Protist* 158:89–103.
- Krishnan NM, Rao BJ. 2009. A comparative approach to elucidate chloroplast genome replication. *BMC Genomics* 10:237–237.
- Lilly JW, Havey MJ, Jackson SA, Jiang J. 2001. Cytogenomic analyses reveal the structural plasticity of the chloroplast genome in higher plants. *Plant Cell* 13:245–254.
- Majeed W, Zhang Y, Xue Y, Ranade S, Blue RN, Wang Q, He Q. 2012. RpaA regulates the accumulation of monomeric photosystem I and PsbA under high light conditions in *Synechocystis* sp. PCC 6803. *PLoS One* 7:e45139.
- Maréchal A, Brisson N. 2010. Recombination and the maintenance of plant organelle genome stability. *New Phytol.* 186:299–317.
- Matsuzaki M, Kikuchi T, Kita K, Kojima S, Kuroiwa T. 2001. Large amounts of apicoplast nucleoid DNA and its segregation in *Toxoplasma gondii*. *Protoplasts* 218:180–191.
- Maul JEJ, Lilly JJW, Cui L, DePamphilis CW, Miller W, Harris EH, Stern DB. 2002. The *Chlamydomonas reinhardtii* plastid chromosome: islands of genes in a sea of repeats. *Plant Cell* 14:2659–2679.
- Mazor Y, Greenberg I, Toporik H, Beja O, Nelson N. 2012. The evolution of photosystem I in light of phage-encoded reaction centres. *Philos Trans R Soc Lond B Biol Sci.* 367:3400–3405.
- Merendino L, Perron K, Rahire M, Howald I, Rochaix J-D, Goldschmidt-Clermont M. 2006. A novel multifunctional factor involved in trans-splicing of chloroplast introns in *Chlamydomonas*. *Nucleic Acids Res.* 34:262–274.
- Moore RB, Oborník M, Janouškovec J, et al. (14 co-authors). 2008. A photosynthetic alveolate closely related to apicomplexan parasites. *Nature* 451:959–963.
- Nelson MJ, Dang Y, Filek E, Zhang Z, Yu VWC, Ishida K, Green BR. 2007. Identification and transcription of transfer RNA genes in dinoflagellate plastid minicircles. *Gene* 392:291–298.
- Nelson N, Yocum CF. 2006. Structure and function of photosystems I and II. *Annu Rev Plant Biol.* 57:521–565.
- Nosek J, Tomáška L, Kucejová B. 2004. The chromosome end replication: lessons from mitochondrial genetics. *J Appl Biomed.* 2:71–79.
- Oborník M, Janouškovec J, Chrudimský T, Lukeš J. 2009. Evolution of the apicoplast and its hosts: from heterotrophy to autotrophy and back again. *Int J Parasitol.* 39:1–12.
- Oborník M, Modrý D, Lukeš M, Černotíková-Stříbrná E, Cihlář J, Tesárová M, Kotabová E, Vancová M, Prášil O, Lukeš J. 2012. Morphology, ultrastructure and life cycle of *Vitrella brassicaformis* n. sp., n. gen., a novel chromerid from the Great Barrier Reef. *Protist* 163:306–323.
- Oldenburg DJ, Bendich AJ. 2004. Most chloroplast DNA of maize seedlings in linear molecules with defined ends and branched forms. *J Mol Biol.* 335:953–970.
- Palmer J. 1983. Chloroplast DNA exists in two orientations. *Nature* 301:92–93.
- Quigg A, Kotabová E, Jarešová J, Kaňa R, Šetlík J, Šedivá B, Komárek O, Prášil O. 2012. Photosynthesis in *Chromera velia* represents a simple system with high efficiency. *PLoS One* 7:e47036.
- Rekosh DM, Russell WC, Bellet AJ, Robinson AJ. 1977. Identification of a protein linked to the ends of adenovirus DNA. *Cell* 11:283–295.
- Ruf S, Kössel H, Bock R. 1997. Targeted inactivation of a tobacco intron-containing open reading frame reveals a novel chloroplast-encoded photosystem I-related gene. *J Cell Biol.* 139:95–102.
- Scharff LB, Koop H-U. 2006. Linear molecules of tobacco ptDNA end at known replication origins and additional loci. *Plant Mol Biol.* 62:611–621.
- Schmidt HA, Strimmer K, Vingron M, von Haeseler A. 2002. TREE-PUZZLE: maximum likelihood phylogenetic analysis using quartets and parallel computing. *Bioinformatics* 18:502–504.
- Schubert WD, Klukas O, Saenger W, Witt HT, Fromme P, Krauss N. 1998. A common ancestor for oxygenic and anoxygenic photosynthetic systems: a comparison based on the structural model of photosystem I. *J Mol Biol.* 280:297–314.
- Sobotka R, Duhring U, Komenda J, Peter E, Gardian Z, Tichy M, Grimm B, Wilde A. 2008. Importance of the cyanobacterial Gun4 protein for chlorophyll metabolism and assembly of photosynthetic complexes. *J Biol Chem.* 283:25794–25802.
- Tomáška L, Makhov AM, Griffith JD, Nosek J. 2002. t-Loops in yeast mitochondria. *Mitochondrion* 1:455–459.
- Tomáška L, Nosek J, Fukuhara H. 1997. Identification of a putative mitochondrial telomere-binding protein of the yeast *Candida parapsilosis*. *J Biol Chem.* 272:3049–3056.
- Vondrušková E, van den Burg J, Zíková A, Ernst NL, Stuart K, Benne R, Lukeš J. 2005. RNA interference analyses suggest a transcript-specific regulatory role for mitochondrial RNA-binding proteins MRP1 and MRP2 in RNA editing and other RNA processing in *Trypanosoma brucei*. *J Biol Chem.* 280:2429–2438.
- Wang Y, Morse D. 2006. Rampant polyuridylation of plastid gene transcripts in the dinoflagellate *Lingulodinium*. *Nucleic Acids Res.* 34:613–619.
- Westhoff P, Alt J, Nelson N, Bottomley W, Bünemann H, Herrmann RG. 1983. Genes and transcripts for the P700 chlorophyll a apoprotein and subunit 2 of the photosystem I reaction center complex from spinach thylakoid membranes. *Plant Mol Biol.* 2:95–107.
- Williamson DH, Denny PW, Moore PW, Sato S, McCready S, Wilson RJ. 2001. The in vivo conformation of the plastid DNA of *Toxoplasma gondii*: implications for replication. *J Mol Biol.* 306:159–168.
- Williamson DH, Preiser PR, Moore PW, McCready S, Strath M, Wilson RJM. 2002. The plastid DNA of the malaria parasite *Plasmodium falciparum* is replicated by two mechanisms. *Mol Microbiol.* 45:533–542.
- Wittig I, Schägger H. 2008. Features and applications of blue-native and clear-native electrophoresis. *Proteomics* 8:3974–3990.
- Woehle C, Dagan T, Martin WF, Gould SB. 2011. Red and problematic green phylogenetic signals among thousands of nuclear genes from the photosynthetic and apicomplexa-related *Chromera velia*. *Genome Biol Evol.* 3:1220–1230.
- Zhang Z, Cavalier-Smith T, Green BR. 2001. A family of selfish minicircular chromosomes with jumbled chloroplast gene fragments from a dinoflagellate. *Mol Biol Evol.* 18:1558–1565.
- Zhang Z, Green BR, Cavalier-Smith T. 1999. Single gene circles in dinoflagellate chloroplast genomes. *Nature* 400:155–159.